

Modelling Class 1 AVO responses of a three layer system

Arnim B. Haase

ABSTRACT

Class 1 three-layer model AVO-responses are computed by a method developed from the Ewing-algorithm for point sources in layered media. Plane-wave and spherical-wave AVO-responses are obtained for a 50 m / 100 m reservoir layer embedded between two semi-infinite layers. Frequency-domain comparisons clearly show reverberations at normal incidence but are not very conclusive for non-zero offset because of these reverberations. Time-domain displays are more revealing in that they show gradual phase changes in the reservoir bottom reflection and, for the 50 m reservoir, even a hint of far-offset tuning.

INTRODUCTION

AVO-responses are traditionally investigated with linear approximations to the Zoeppritz equations. Small parameter changes are commonly assumed for these approximations, and they tend to break down near critical angles where incidence angles are no longer small. Applying “*true Zoeppritz*” is still just a plane-wave approximation to the real world. Spherical-wave analysis utilizing Weyl/Sommerfeld integrals opens up the potential of log-offset amplitudes (Haase and Ursenbach, 2006; Ursenbach et al., 2007). All these investigations are based on two-layer models. Downton and Lines (2002) mention offset dependent tuning as a challenge to real-data AVO-inversion. This study goes beyond the two-layer case of Weyl/Sommerfeld integral computations to investigate tuning phenomena. The Ewing-algorithm for point sources in layered media utilized in this study is introduced elsewhere (Haase, 2008, this Volume).

PLANE-WAVE RESPONSES OF A THREE-LAYER MODEL

The model used in this report consists of a reservoir layer (Layer 2) with finite thickness, embedded between two semi-infinite layers (Layer 1 and Layer 3) with identical rock properties:

$$\alpha_1 = \alpha_3 = 2000 \text{ m/s} ,$$

$$\beta_1 = \beta_3 = 879.88 \text{ m/s} ,$$

$$\rho_1 = \rho_3 = 2400 \text{ kg/m}^3 ,$$

$$\alpha_2 = 2933.33 \text{ m/s} ,$$

$$\beta_2 = 1882.29 \text{ m/s} ,$$

$$\rho_2 = 2000 \text{ kg/m}^3 .$$

These parameters describe a Class 1 AVO anomaly (Haase and Ursenbach, 2006) that has a zero-offset/angle P-wave reflectivity of $R_{pp} = 0.1$. Figure 1 demonstrates the frequency dependence of this plane-wave Class 1 vertical incidence P-wave reflection coefficient,

given a reservoir (Layer 2) thickness of 100 m. Also plotted is the normal incidence P-wave reflection coefficient of the comparable one-interface (two-layer) situation.

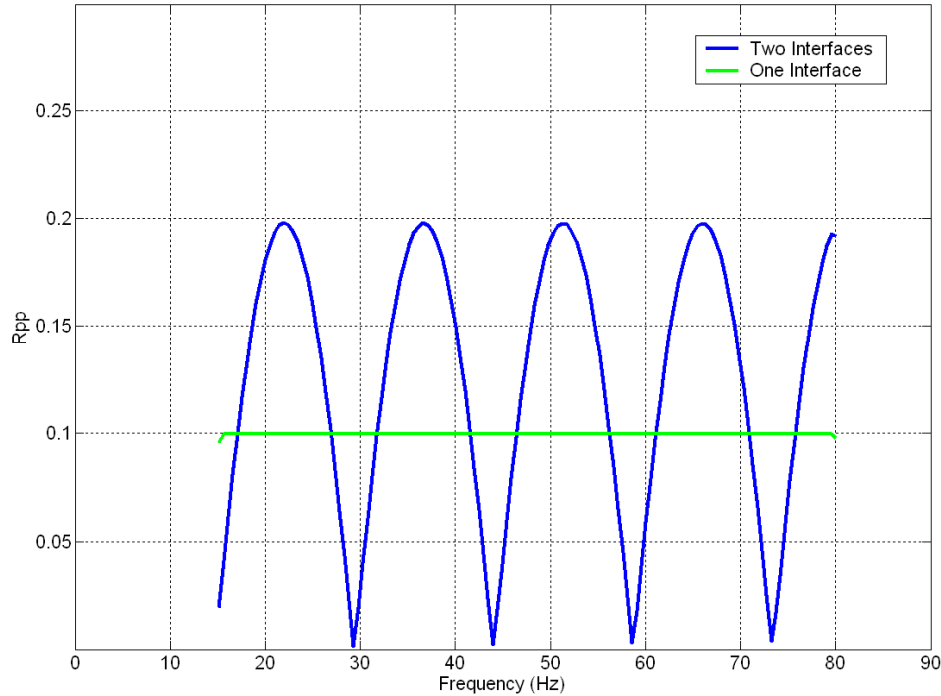


FIG. 1. AVO Class 1 plane-wave PP reflection coefficient at vertical incidence as a function of frequency (100 m reservoir).

The notching and peaking of this three-layer P-wave reflection coefficient ($R_{pp3}(\omega)$) observed in Figure 1 is evidence for reservoir-layer reverberations in a plane-wave normal incidence case. The first notch is to be expected at a frequency where the total reservoir-layer travel distance of 200 m (twice the reservoir-thickness of 100 m) equals the wavelength λ according to

$$\alpha = \lambda f \quad \text{giving (with the velocity } \alpha_2 \text{ specified above)}$$

$$f_{n1} = \alpha_2 / \lambda = (2933.33 \text{ m/s}) / (200 \text{ m}) = 14.667 \text{ Hz} .$$

Note the P-wave velocity inversion at the second interface (Layer 2 to Layer 3). Notching is repeated at multiples of f_{n1} where an integer multiple of wavelengths λ fits into the total reservoir-layer travel distance of 200 m. That means

$$f_{n2} = 2 f_{n1} = 29.333 \text{ Hz} ,$$

$$f_{n3} = 3 f_{n1} = 44 \text{ Hz} ,$$

$$f_{n4} = 4 f_{n1} = 58.667 \text{ Hz} \text{ and so on.}$$

Peaks of $R_{pp3}(\omega)$ occur at points of $n f_{n1} / 2$ for odd $n = 1, 3, 5 \dots$. $R_{pp3}(\omega)$ for a 50 m reservoir can be seen in Figure 2 (all other parameters are identical to Figure 1).

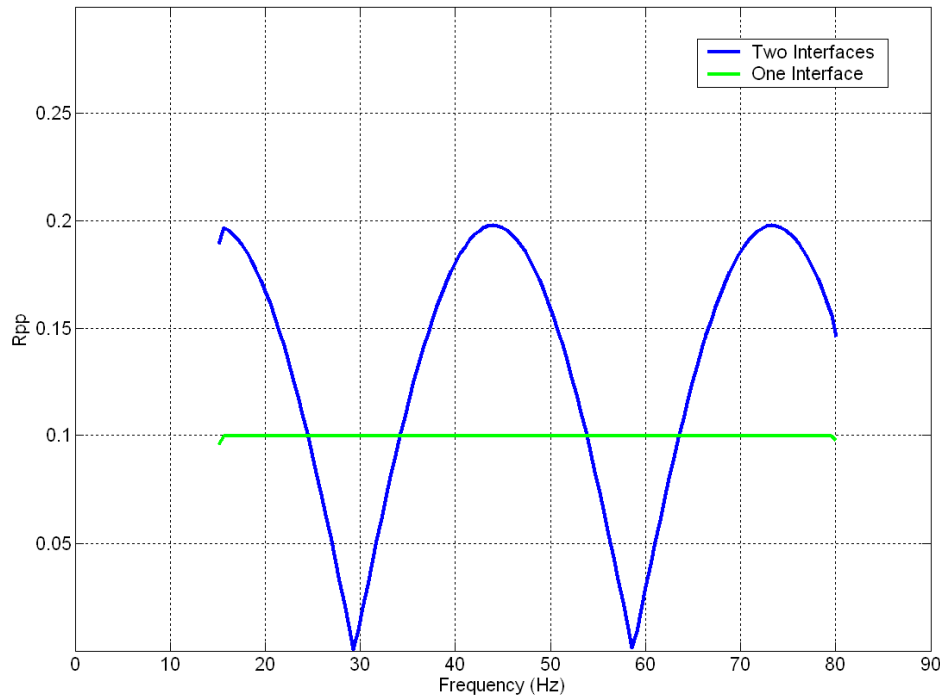


FIG. 2. AVO Class 1 plane-wave PP reflection coefficient at vertical incidence as function of frequency (50 m reservoir).

The first notch for a 50 m reservoir occurs at

$$f_{na} = \alpha_2 / \lambda = (2933.33 \text{ m/s}) / (100 \text{ m}) = 29.333 \text{ Hz} ,$$

with the second one at

$$f_{nb} = 2 f_{na} = 58.667 \text{ Hz} \text{ and so on.}$$

The influence of reverberations is visible in both, Figure 1 and Figure 2. Clearly, plane-wave zero-offset $R_{pp3}(\omega)$ depends on reservoir-thickness as was to be expected.

What would be the three-layer plane-wave AVO-response for non-zero offset? Figure 3 (for a 100 m reservoir) and Figure 4 (for a 50 m reservoir) answer this question. Zero-offset responses equivalent to Figures 1 and 2 can be found at the left-hand side of Figures 3 and 4. A single interface Class 1 plane-wave comparison can be found in Figure 5. Reservoir-layer reverberations are obscuring the true AVO-response even in this noise free plane-wave situation. Sommerfeld integrals are employed next to investigate time-domain and frequency-domain spherical-wave responses of three-layer cases modelling a Class 1 reservoir.

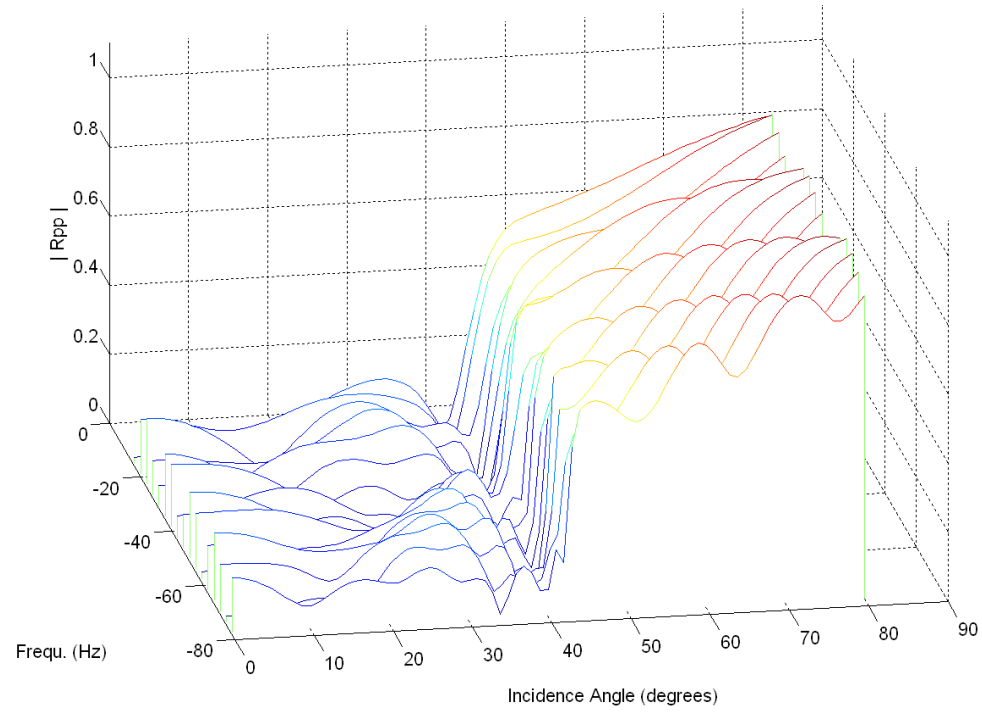


FIG. 3. AVO-Class 1 plane-wave PP reflection coefficient (100 m reservoir).

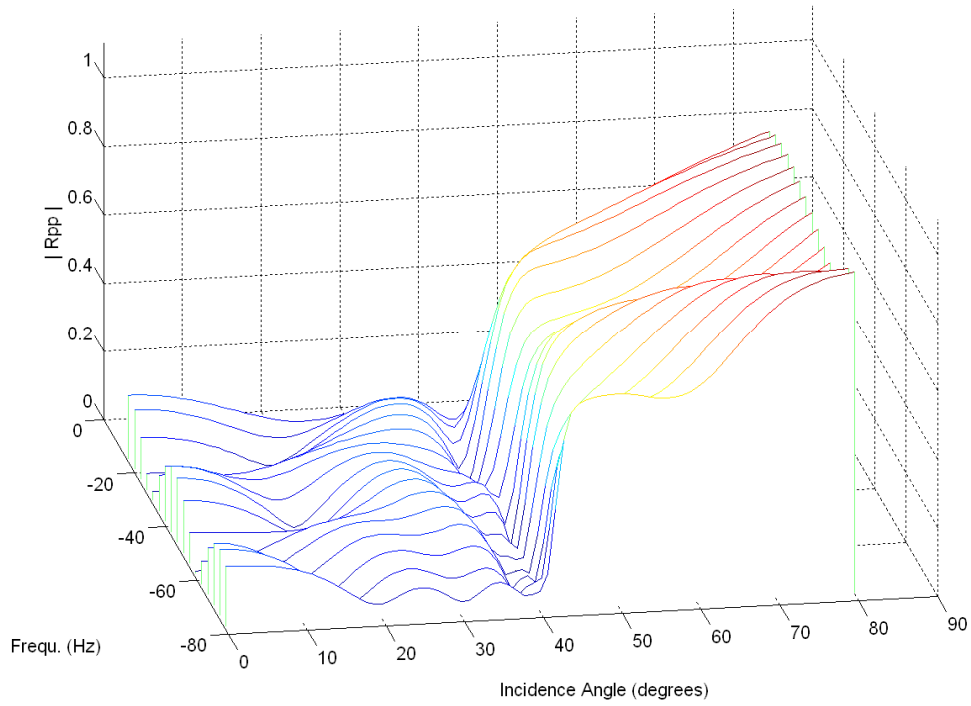


FIG. 4. AVO-Class 1 plane-wave PP reflection coefficient (50 m reservoir).

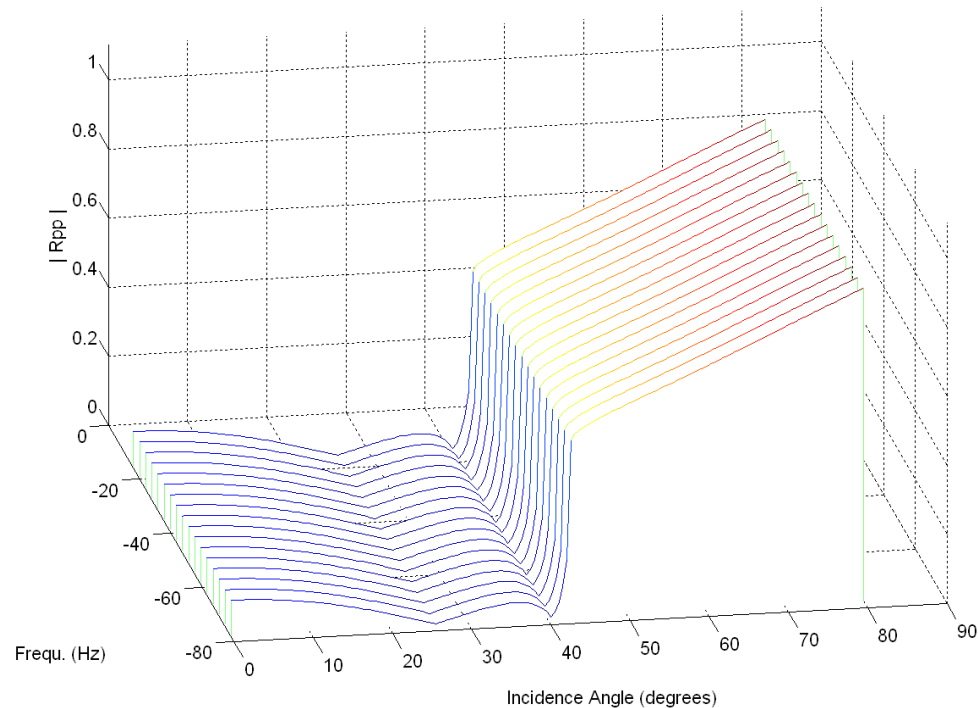


FIG. 5. AVO-Class 1 plane-wave PP reflection coefficient (single-interface).

SPHERICAL-WAVE RESPONSES OF A THREE-LAYER MODEL

The model utilized for spherical-wave computations has the same rock properties and geometry as introduced in the previous section. The depth z of the first interface below a P-wave point source must also be specified. The reservoir model of Haase and Ursenbach (2006) assumes a source-to-interface reference depth of 500 m, and that value for depth z shall be adopted here as well. Displayed in Figure 6 is the frequency dependence of a spherical-wave Class 1 vertical incidence P-wave reflection coefficient for a reservoir-thickness of 100 m. This is the spherical-wave equivalent to the plane-wave result in Figure 1. A zero-offset spherical-wave response for the 50 m reservoir, with all other parameters identical to the 100 m case above, can be seen in Figure 7 which may be compared to the plane-wave situation in Figure 2. At normal incidence no differences are expected between plane-wave and spherical-wave computations. However, close inspection of Figures 6 and 7 reveals a general trend of reflection coefficient magnitudes diminishing with frequency which is not present in the plane-wave comparisons given in Figures 1 and 2. One possible explanation is the role of near-field effects. Not only does near-field strength diminish with increasing distance from the source, but it also diminishes with increasing frequencies (Haase and Stewart, 2008, this Volume). Even at 500 m reservoir depth there is a frequency dependent remnant near-field.

Three-layer spherical-wave Class 1 AVO-responses for non-zero offsets are shown in Figure 8 (for a 100 m reservoir) and Figure 9 (for a 50 m reservoir).

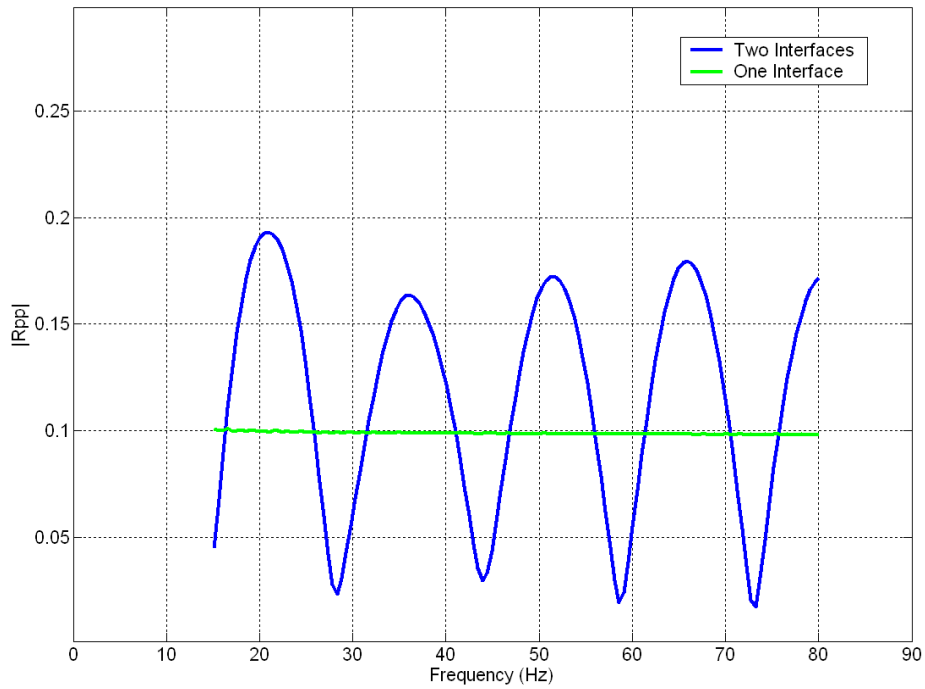


FIG. 6. AVO Class 1 spherical-wave PP reflection coefficient at vertical incidence as a function of frequency (100 m reservoir).

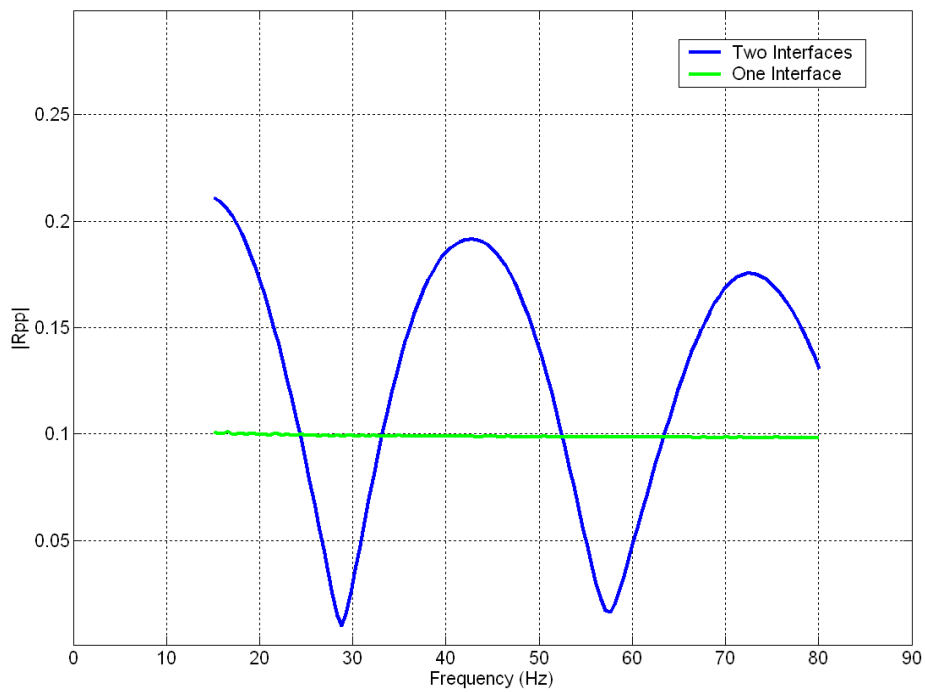


FIG. 7. AVO Class 1 spherical-wave PP reflection coefficient at vertical incidence as a function of frequency (50 m reservoir).

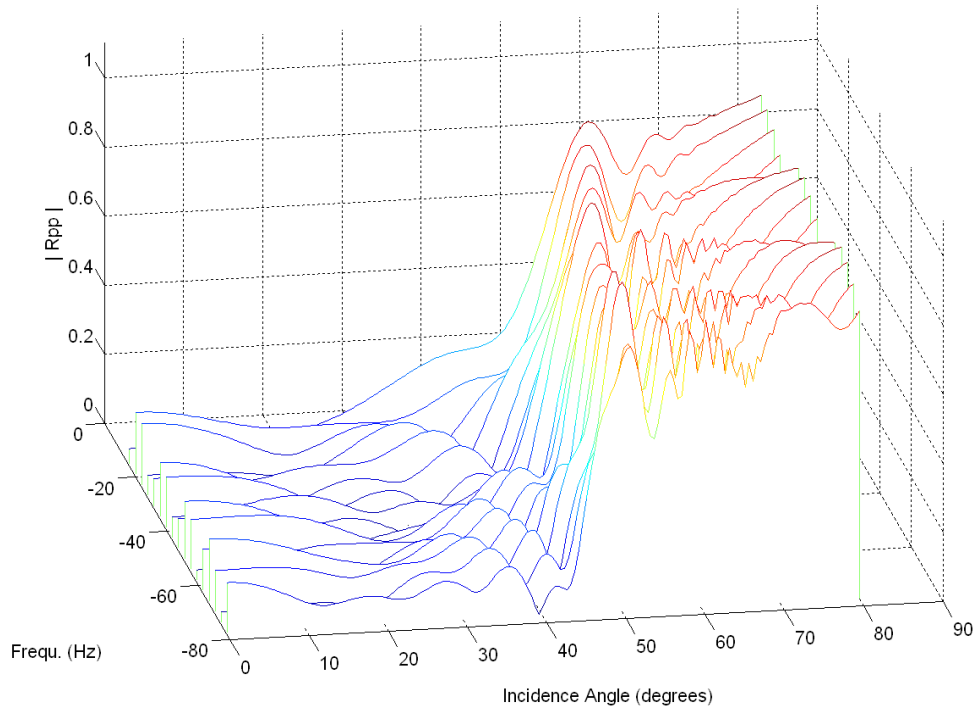


FIG. 8. AVO-Class 1 spherical-wave PP reflection coefficient (100 m reservoir).

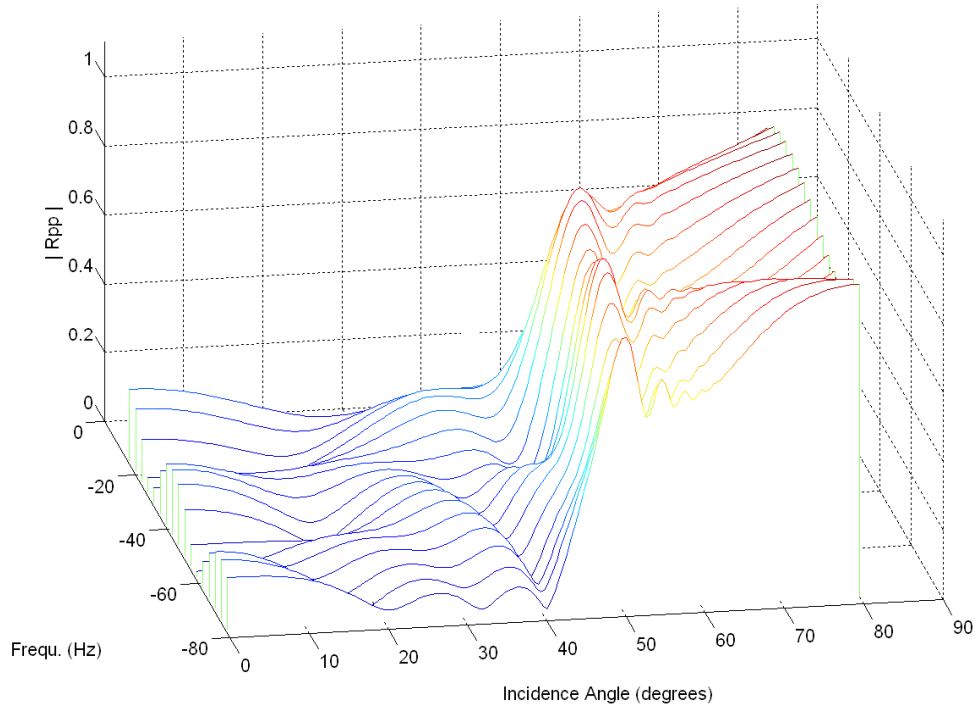


FIG. 9. AVO-Class 1 spherical-wave PP reflection coefficient (50 m reservoir).

As in the plane-wave comparisons of Figures 3 and 4, reservoir-layer reverberations are obscuring the AVO-response. There are, however, differences in detail, especially at low frequencies away from zero-offset/zero-incidence angles, and just beyond the critical angle of 43° . Figure 10 shows a Class 1 spherical-wave AVO-response without reverberations because of a semi-infinite reservoir-layer. When comparing to the plane-wave equivalent plotted in Figure 5, low-frequency AVO differences and high-incidence angle AVO differences become a little clearer.

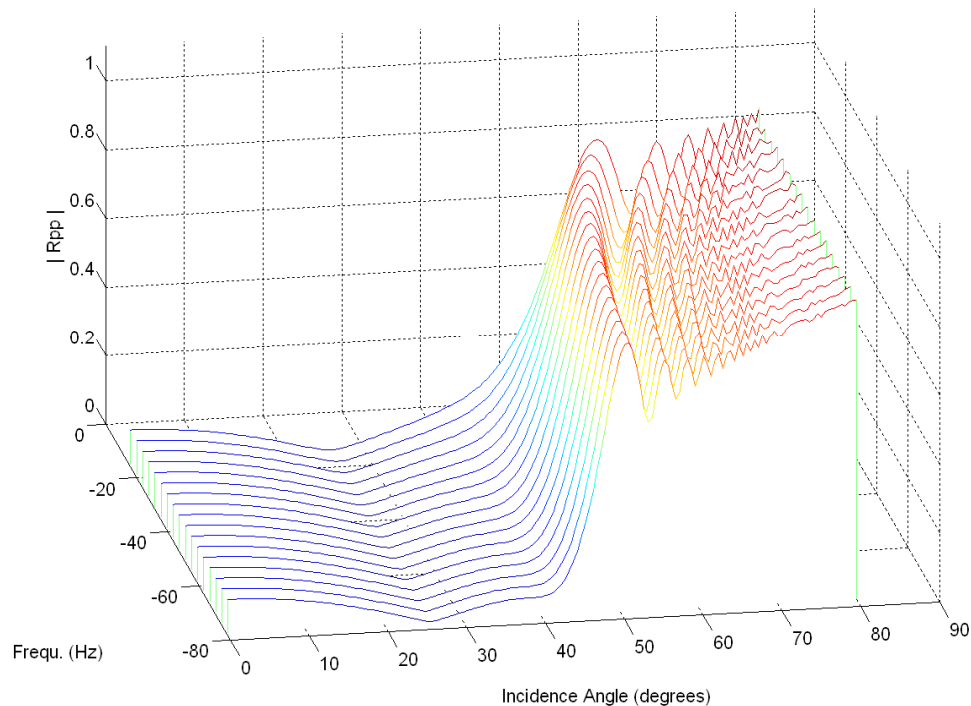


FIG. 10. AVO-Class 1 spherical-wave PP reflection coefficient (single-interface).

An inverse Fourier-transform of all the frequency components from which the magnitude display of Figure 10 is derived results in the trace plot of Figure 11. The ringing of the employed Ormsby wavelet (5/15-80/100 Hz) is apparent. Also clearly visible is a wavelet polarity change between 25° and 26° of incidence (angle to the vertical). This kind of “zero-crossing” is typical for a Class 1 AVO-response. Note that in this trace plot (and in the following two as well) the maximum incidence angle displayed is 32° which is short of the 43° critical angle dictated by the chosen model parameters. From an inverse Fourier-transform of the input to Figure 8, the trace display of Figure 12 is obtained. Reservoir-thickness for this example is 100 m, and the reservoir bottom reflection shows a polarity reversal because of the P-wave velocity inversion at that interface. The reservoir bottom reflection displays a more gradual phase rotation rather than a “zero-crossing”. The 50 m reservoir equivalent to Figure 12 can be seen in Figure 13. As expected, the two reservoir reflections moved closer in time because the now shallower bottom reflection arrives at an earlier time in Figure 13. The gradual phase rotation of the second reflection is more noticeable than in Figure 12, and there is also a “hint” of amplitude built-up because of far-offset tuning in Figure 13.

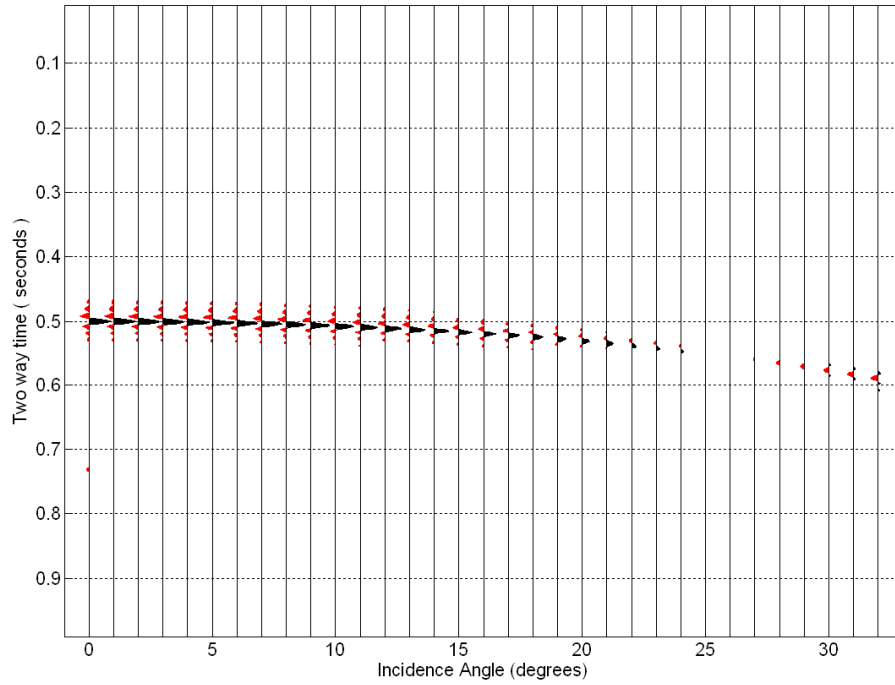


FIG. 11. Class 1 spherical-wave PP reflection traces (single-interface at z=500 m).

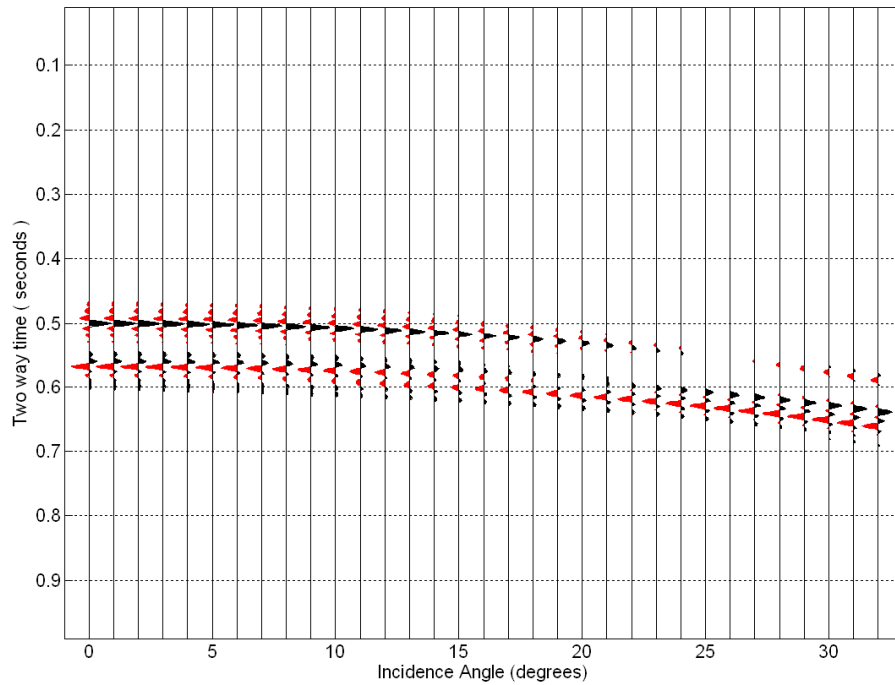


FIG. 12. Class 1 spherical-wave PP reflection traces for a 100 m reservoir (top at z=500 m).

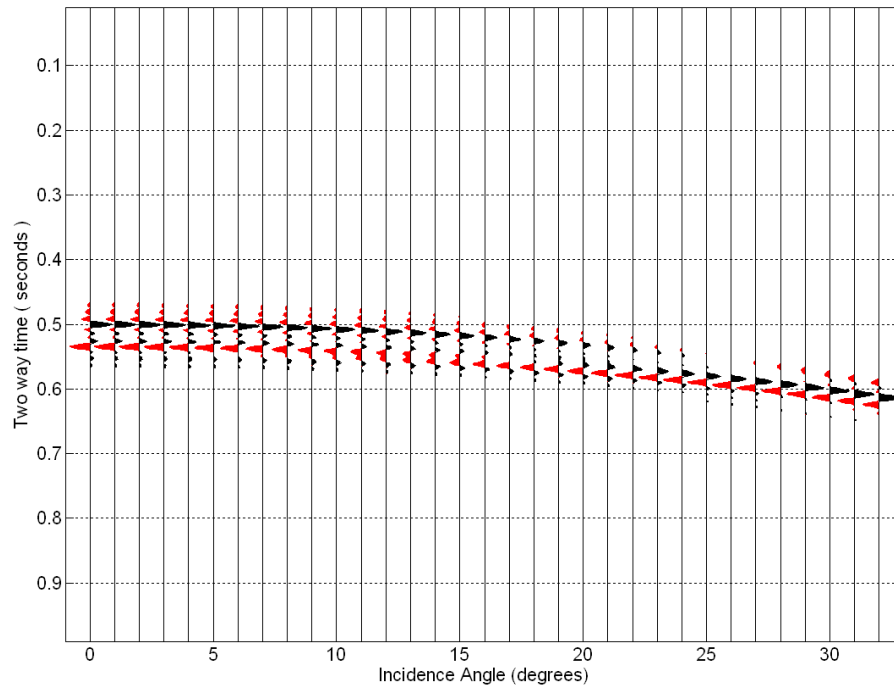


FIG. 13. Class 1 spherical-wave PP reflection traces for a 50 m reservoir (top at $z=500$ m).

It can be expected that, depending on rock property contrasts, the AVO-response of a system with more and/or thinner layers might not at all look like the “textbook example” of Figure 11.

CONCLUSIONS

A computational method based on the Ewing-algorithm for point sources in layered media is employed to obtain a three-layer model AVO-response. The rock properties chosen for two semi-infinite embedding layers and the reservoir layer wedged in-between lead to a Class 1 AVO-response from the top interface. Plane-wave and spherical-wave model responses for reservoir thicknesses of 50 m and 100 m are computed and compared. Reservoir layer reverberations are investigated by analyzing zero-offset (normal-incidence) AVO-responses. Not surprisingly, the pattern of these reverberations is controlled by reservoir thickness. Frequency-domain comparisons between non-zero offset plane-wave and spherical-wave three-layer AVO model responses are not very conclusive because reservoir layer reverberations obscure the picture. The plots of time-domain traces (obtained by inverse Fourier-transform of computed frequency points) are more revealing. They show a reflection each off the top and off the bottom of the reservoir. The smaller the reservoir thickness the more closely spaced are these two reflections. The deep reflector response shows a gradual phase rotation but no zero-crossing in the incidence angle range analyzed. The top reflector response displays a zero-crossing which is characteristic for Class 1 AVO.

ACKNOWLEDGEMENTS

Support from the CREWES Project at the University of Calgary and its industrial sponsorship is gratefully acknowledged.

REFERENCES

- Downton, J.E., and Lines, L.R., 2002, AVO NMO: CREWES Research Report, **14**.
- Haase, A.B., and Ursenbach, C.P., 2006, Spherical-wave AVO modelling in elastic and anelastic media: CREWES Research Report, **18**.
- Haase, A.B., and Stewart, R.R., 2008, Modelling near-field effects in VSP-based Q-estimation: CREWES Research Report, **20**.
- Haase, A.B., 2008, Extending Sommerfeld-integral based spherical wave field computations beyond two layers: CREWES Research Report, **20**.
- Ursenbach, C.P., Haase, A.B., and Downton, J.E., 2007, An efficient method for AVO modeling of reflected spherical waves: *Journal of Seismic Exploration*, **16**, 79-104.